Bulletin of Electrical Engineering and Informatics
Vol. 15, No. 6, December 2026, pp. 4912~4923
ISSN: 2302-9285, DOI: 10.11591/eei.v15i6.12601

LPC-based efficient compression of phonocardiogram signals for IoT-enabled cardiac monitoring systems

Samer Alabed[1], Mohammad Al-Rabayah[2], Omar M. Bwaliez[3]
[1]Department of Biomedical Engineering, School of Applied Medical Sciences, German Jordanian University, Amman, Jordan
[2]College of Engineering and Technology, American University of the Middle East, Egaila, Kuwait
[3]Department of Management Sciences, Business School, German Jordanian University, Amman, Jordan

Article Info

Article history:

Received Feb 21, 2026
Revised Aug 25, 2026
Accepted Sep 4, 2026

Keywords:

Cardiovascular disease
Good health and well-being
Internet of things
Linear predictive coding
Phonocardiogram
Sustainable healthcare system
Wearable medical devices

ABSTRACT

This study proposes an efficient linear predictive coding (LPC)-based compression method for phonocardiogram (PCG) signals targeting real-time cardiac monitoring applications. The proposed approach models each PCG frame using LPC to capture its spectral characteristics and represents the remaining information through a residual signal. An adaptive thresholding parameter is applied to the residual to adjust the compression level. By varying this parameter, the proposed framework provides a flexible compression ratio (CR) ranging from approximately 4:1 to 30:1, while maintaining good reconstruction quality and preserving the essential morphology and characteristics of the PCG waveform. The LPC parameters and non-zero residual components are quantized and transmitted to enable signal reconstruction at the decoder. Experimental results demonstrate that this approach can substantially reduce the amount of transmitted PCG data while maintaining high-quality reconstructed signals. The proposed framework therefore provides a computationally efficient and flexible low-bitrate solution for resource-constrained biomedical and remote cardiac monitoring applications.

This is an open access article under the CC BY-SA license.

Corresponding Author:

Samer Alabed
Department of Biomedical Engineering, School of Applied Medical Sciences
German Jordanian University
Amman 11180, Jordan
Email: samer.alabed@gju.edu.jo

1. INTRODUCTION

Biomedical signal processing of phonocardiogram (PCG) signals plays a vital role in continuous cardiac assessment by capturing the acoustic reflections of structural and hemodynamic heart valve movements, primarily the first (S_1) and second (S_2) heart sounds [1]–[3]. Traditional auscultation using stethoscopes [4], [5] faces practical drawbacks, including unrecorded events and subjective assessment, making continuous digital monitoring indispensable. With the rapid deployment of telemedicine, internet of things (IoT) frameworks, and remote patient monitoring [6]–[9], transmitting continuous PCG recordings has become critical for decentralized healthcare. However, the continuous streaming of acoustic cardiac data generates substantial data volumes that strain communication bandwidth and exhaust battery resources in wearable sensors, creating an urgent demand for advanced source coding and communication strategies [10]–[20] that reduce bitrates while preserving vital diagnostic integrity. The primary technical challenge in PCG compression lies in achieving a high compression ratio (CR) without sacrificing transient, low-amplitude diagnostic features such as pathological murmurs and subtle valve clicks. Unlike electrocardiograms (ECG) [21]–[25], which depict electrical activity, acoustic PCG waveforms exhibit severe amplitude variability,

background acoustic interference, and non-stationary valve closures that complicate data reduction while preserving clinical features [4], [26]–[28]. Existing PCG compression schemes present notable trade-offs across current literature. Lossless and transform-based methods, such as the wavelet transform, Huffman coding, and run-length encoding [13]–[16], [20]–[22], [29], effectively isolate sub-band components and retain complete information integrity, but their heavy buffering overhead and low CR restrict battery longevity. Conversely, predictive coding [30]–[34] and emerging deep autoencoder models achieve higher data reduction by learning complex signal patterns; however, neural approaches demand heavy matrix computations that exceed edge microcontrollers, while standard predictive schemes suffer from synthesis filter instability under direct coefficient quantization and insufficient residual compression. Consequently, a critical research gap remains for an ultra-low-complexity PCG compression scheme that simultaneously guarantees filter stability, delivers high CR, and operates without heavy transform or neural computational overhead. To bridge this gap, this paper proposes an efficient, low-cost PCG compression framework that integrates short-time linear predictive coding (LPC) with line spectral frequency (LSF) parameterization and adaptive residual thresholding. The explicit contributions of this work are threefold: first, formulating a quasi-stationary short-time framing strategy to extract the acoustic spectral envelope without autocorrelation distortion; second, utilizing LSF parameterization to guarantee synthesis filter stability under coarse quantization; and third, applying an adaptive energy threshold to prune redundant excitation samples while preserving essential cardiac morphology. Experimental evaluations show that the proposed framework achieves an average CR of 20 with high signal fidelity, confirming its practical significance for real-time cardiac telemonitoring on resource-constrained IoT platforms.

2. METHOD

The proposed PCG signal compression framework is implemented via an encoder-decoder architecture, as illustrated in the system model in Figure 1. The encoding pipeline, depicted in Figure 1(a), accepts the discrete input PCG waveform $c[n]$, divides it into short-time frames, and processes each frame through the analysis filter $G(z)$ to generate the prediction residual signal $e[n]$. This stage encompasses initial signal preprocessing (framing, windowing, bandpass filtering, and normalization) and LPC parameter estimation to model the spectral envelope. Conversely, the decoding pipeline, shown in Figure 1(b), reconstructs the PCG waveform using the synthesis filter $H(z) = 1/G(z)$ excited by the transmitted residual signal $\hat{e}[n]$ and then concatenates the frames to get the estimated PCG signal. To optimize transmission bandwidth for resource-constrained biomedical devices, both the LPC coefficients and the non-zero residual components are quantized prior to reconstruction.

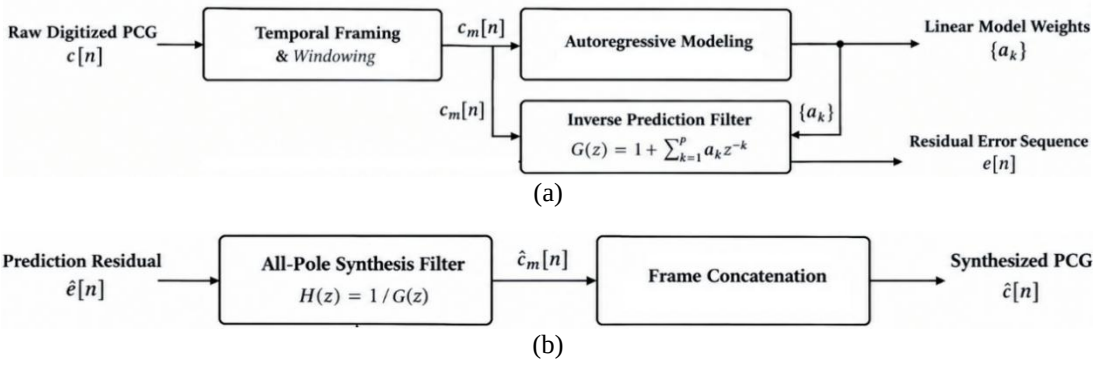


Figure 1. Block diagram of the system model with; (a) encoding and (b) decoding pipelines

2.1. Preliminary phonocardiogram signal conditioning

Raw PCG recordings are first normalized to zero-mean and unit-variance to eliminate baseline offsets, followed by digital low-pass filtering to suppress high-frequency noise while preserving diagnostic acoustic bands, and segmented into quasi-stationary frames using a Hanning window to mitigate spectral leakage and optimize short-time linear prediction efficiency, with synthetic Gaussian noise addition strictly documented as an optional controlled sensitivity test.

2.2. Autoregressive modeling and parameter estimation

The main idea of this method is to make a predictive model of each part of the PCG signal by using

previous values of the sample, which gives an estimated representation of the signal. The residual or remaining signal is obtained by finding out how much the observed signal and its predicted counterpart differ from each other. This means that instead of keeping or sending the whole PCG signal, just the considerably compressed residual part can be encoded and sent. In decoding process, the decoder uses the compressed residual signal together with a synthesis filter that has the same coefficients as those obtained during the prediction phase. If the residual signal is deteriorated or if the filter characteristics are not ideal, the reconstructed output will not fully correspond to the original signal. The mathematical framework that supports this method [10] gives formal definitions for both the predicted and residual signals through (1) and (2):

$$\hat{c}(n) = \mathrm{a}^T \mathrm{c}_{n-1} \tag{1}$$

$$e(n) = c(n) - \mathrm{a}^T \mathrm{c}_{n-1} \tag{2}$$

The discrete PCG acoustic sample $c(\mathrm{n})$ is estimated via forward linear prediction as $\hat{c}(\mathrm{n})$ computed from the inner product of the optimal weighting vector $\mathrm{a} = [\mathrm{a}_1, \ldots, \mathrm{a}_\mathrm{p}]^\mathrm{T}$ and past state vector $\mathrm{c}_{\mathrm{n}-1} = [c(\mathrm{n}-1), \ldots, c(\mathrm{n}-\mathrm{p})]^\mathrm{T}$, where p is the model order and $(\cdot)^\mathrm{T}$ denotes matrix transposition. The resulting residual sequence $e(\mathrm{n})$ represents the prediction error after removing the component explained by the linear predictor and therefore provides the signal component used for subsequent residual processing. Over a localized frame of duration L_s with sample index $n \in \{0, \ldots, L_s - 1\}$, the cumulative average squared prediction error functional $\mathcal{Q}$ is defined via the squared Euclidean norm $\| \cdot \|_2^2$ as (3):

$$\mathcal{Q} = \frac{1}{L_s} \|\mathrm{e}\|_2^2 \tag{3}$$

where $e = [e[0], e[1], \ldots, e[L_s - 1]]^T$. Minimizing $\mathcal{Q}$ by setting the gradient vector $\nabla_\mathrm{a} \mathcal{Q} = 0_\mathrm{p}$ yields the standard Yule-Walker normal as (4) [10]:

$$\mathrm{R}_{cc}\, \mathrm{a} = -\mathrm{r}_{cc} \tag{4}$$

where 0_p is a length-p zero vector and $\mathrm{r}_{\mathrm{cc}} = [r_{cc}(1), \ldots, r_{cc}(p)]^\mathrm{T}$ is the cross-correlation lag vector, and R_{cc} is the symmetric positive-definite Toeplitz autocorrelation matrix formed by sequence entries $r_{cc}(k) = \sum_\mathrm{n} c(n)c(n-k)$ at $k = |l - i|$ [10]. Setting $a_0 = a_p(0) = 1$ defines the augmented parameter vector $\tilde{\mathrm{a}} = [\mathrm{a}^\mathrm{T}, 1]^\mathrm{T}$ and expanded matrix $\hat{\mathrm{R}}_{cc}$, unifying the system into the homogeneous relation:

$$\hat{R}_{cc}\, \tilde{\mathrm{a}} = \begin{bmatrix} 0_\mathrm{p} \\ Q_m \end{bmatrix} \tag{5}$$

The minimum attainable residual mean-square error $\mathrm{Q}_\mathrm{m} = \min[\mathcal{Q}]$ is given by the cross-correlation projection [10]:

$$Q_m = \frac{1}{L_s} [r_{cc}(0) + r_{cc}^T\, a] \tag{6}$$

2.3. Residual thresholding

A thresholding technique purely keeps the leading amplitude components, taking advantage of the inherent sparsity traits of the residue signal. The threshold parameter θ is set as a proportional part of the peak residual amplitude in each analysis window. The residual signal that is thresholded after this is represented as (7):

$$e_{sparse}(n) = \hat{e}(n) = \begin{cases} e(n), & if\ |e(n)| \geq \theta \\ 0, & otherwise \end{cases} \tag{7}$$

The energy left over is mainly preserved through this selective retention method that uses a smaller number of samples, thus increasing the compression efficiency and keeping the waveform fidelity close to the original with a slight degradation.

2.4. Signal reconstruction

After quantization and communication of LPC parameters and residual parts, the decoder reconstructs the signal using these components. The resulting signal is very similar to the original waveform and has the

important morphological features needed for clinical diagnosis. This method produces a good balance between the two opposing forces, that is, compression efficiency and signal fidelity, which makes it to be of great value in situations where bandwidth and storage capacity are the limiting factors.

2.5. Compact representation and quantization of filter coefficients

Although LPC coefficients can model PCG signals very well, they lose their effectiveness for transmission because they are prone to instability, and cause more quantization errors at lower bit rates due to their higher sensitivity. To solve this problem, the LPC coefficients are changed to LSF coefficients, also known as line spectrum pairs (LSPs). These frequency domain coefficients show excellent stability characteristics and prove to be more resistant to quantization effects, all this while maintaining a one-to-one mathematical relationship with the original LPC coefficients [10]. The LPC analysis (whitening) filter $G_p(z)$, that decorrelates the PCG signal, is parameterized as a finite-impulse response (FIR) operator:

$$G_p(z) = 1 + a^T z_p \tag{8}$$

where $z_p = [z^{-1}, z^{-2}, \dots, z^{-p}]^T$ is the backward delay operator vector in the complex z-domain, and $(\cdot)^T$ represents vector transposition. To extract the LSFs, the system transfer function is projected into two boundary polynomials, denoted as the symmetric component $A(z)$ and antisymmetric component $B(z)$ [10]. Rather than formulating them through boundary polynomial subtraction, they are expressed directly as closed-form z-domain polynomial series with mirror-image reciprocal coefficients:

$$A(z) = \sum_{k=0}^{p+1} (a_k + a_{p+1-k}) z^{-k} \tag{9}$$

$$B(z) = \sum_{k=0}^{p+1} (a_k - a_{p+1-k}) z^{-k} \tag{10}$$

where $k \in \{0, 1, \dots, p+1\}$ indices the spectral delay stages and the boundary termination coefficient is clamped to zero ($a_{p+1} = 0$). The term z^{-k} acts as a discrete k-sample delay operator. Due to the linear cancellation of the complementary cross-terms, the target analysis operator $G_p(z)$ is reconstructed from the dual auxiliary spectra via a parallel feedforward branch [10]:

$$G_p(z) = \frac{1}{2} \sum_{k=0}^{p+1} \left[(a_k + a_{p+1-k}) + (a_k - a_{p+1-k}) \right] z^{-k} = \frac{A(z)+B(z)}{2} \tag{11}$$

For an even prediction memory p, $A(z)$ has a zero at the Nyquist frequency ($z = -1$), whereas $B(z)$ contains a zero at DC ($z = +1$). All other zeros reside on the complex unit perimeter ($|z| = 1$) as conjugate pairs $e^{\pm j\omega_k}$, whose angular arguments $\omega_k \in (0, \pi)$ specify the LSFs. The roots of $A(z)$ and $B(z)$ interlace on the unit circle and their angular positions define the LSFs ($0 < \omega_{A,1} < \omega_{B,1} < \omega_{A,2} < \cdots < \pi$), the inverse all-pole reconstruction operator $H(z) = 1/G_p(z)$ retains guaranteed bounded-input bounded-output stability under parameter quantization. The excitation residual $e(n)$ drives $H(z)$ to synthesize the complete acoustic PCG waveform without boundary discontinuities. The symmetric polynomial $A(z)$ has one real root only, which is z=-1, while the antisymmetric polynomial $B(z)$ has one real root only at z=+1. All the other roots of both polynomials are complex, located on the unit circle and occurring as conjugate pairs. These roots determine the LSFs, which are linked to the angles of the roots in the upper half of the unit circle. The alternating arrangement of these roots is a factor that guarantees the stability of the prediction filter G(z) and, thus, is a crucial condition to be met for the signal to remain undistorted throughout the quantization and reconstruction stages. In the autoregressive coding scheme, PCG waveform resynthesis is performed using an autoregressive reconstruction filter activated by an excitation e(n). The residual part carries the fine scale temporal dynamics and the synthesis filter reconstructs the spectral envelope characteristics. The accurate reconstruction of both components is crucial for the preservation of clinical morphological features of the PCG signal. To obtain a compact and structurally valid representation of the LPC parameters, the normalized LSFs are quantized using an order-preserving adaptive differential quantization scheme. The normalized LSF vector is defined as: $\bar{\omega}_k = \frac{\omega_k}{\pi}$, $0 < \bar{\omega}_1 < \bar{\omega}_2 < \cdots < \bar{\omega}_p < 1$. Instead of quantizing the LSF values or their real-valued differences independently, the ordered LSF vector is first mapped onto a finite uniform lattice containing $Q + 1$ levels. The quantized LSF positions are represented by strictly increasing integer indices $1 \le m_1 < m_2 < \cdots < m_p \le Q - 1$, where $\widehat{\bar{\omega}}_k = \frac{m_k}{Q}$. To avoid transmitting the indices directly, the encoder represents them through positive integer gaps: $d_1 = m_1, d_k = m_k - m_{k-1}, \quad k = 2, \dots, p$, with the additional terminal gap defined as: $d_{p+1} = Q - m_p$. Accordingly, all gap values are positive integers and satisfy the conservation constraint: $\sum_{k=1}^{p+1} d_k =$

Q. This constrained representation guarantees that the reconstructed LSFs remain strictly ordered and within the valid interval $(0,1)$, without requiring post-quantization sorting, coefficient correction, or codebook lookup. The quantization resolution Q and the bit allocation are selected adaptively according to the frame characteristics. More bits are assigned to the LSF regions that exhibit greater spectral sensitivity or contribute more strongly to the representation of the dominant PCG components, particularly the frequency regions associated with the S1 and S2 heart sounds. Conversely, fewer bits are assigned to less sensitive spectral regions. The resulting gap sequence is encoded using bounded integer representation and differential entropy coding, while the frame-dependent scale and quantization parameters are transmitted through a small side-information field. This approach reduces coefficient redundancy, preserves the inherent ordering of the LSFs, and ensures that the reconstructed LPC polynomial can be converted into a valid stable all-pole synthesis filter, provided that the standard LSF-to-LPC conversion is properly applied.

2.6. Suggested compression framework

The suggested system for PCG compression takes up residual thresholding and LSP-based parametric representation and combines them into one LPC-based technique all in one go, that is, the whole process done to reduce the amount of data sent while the PCG signal's morphological aspect stays the same. In an analytical frame, a tenth-order LPC model is applied to produce the predictive coefficients, and the estimated signal is then subtracted from the actual wave to produce the residual error signal. Sparse properties usually characterize this residual and the main part of the values is either close to or exactly zero. As illustrated in Figure 2, the encoder workflow carries out autoregressive modeling, selective error thresholding, and quantization processes to generate an ultra-compact bitstream for each segmented PCG frame. Rather than encoding the full-length residual sequence, a thresholding and pruning operation suppresses near-zero fluctuations and retains only dominant prediction errors, drastically lowering the transmission overhead while preserving crucial diagnostic complexes. Concurrently, the extracted model parameters are quantized alongside the pruned residual symbols before entering a multiplexing stage to form the finalized frame payload.

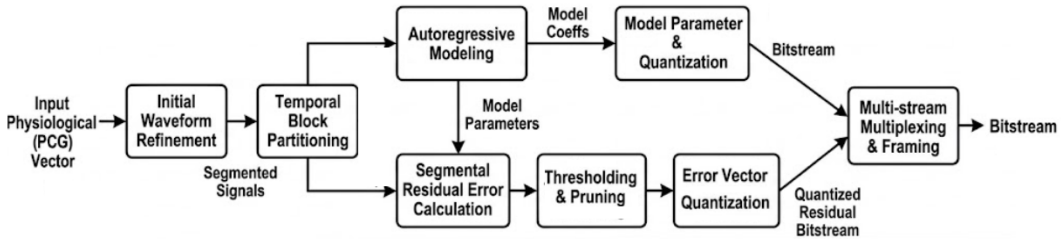


Figure 2. Encoder architecture and processing stages

The decoder stage, depicted in Figure 3, is tasked with synthesizing each PCG frame from the demultiplexed parameter bitstreams and recovered error sequences. The incoming bitstream is demultiplexed to isolate the encoded spectral parameters and residual symbols, which then undergo inverse quantization to restore the physical filter weights and residual driving vector. These restored driving samples excite the all-pole inverse filter, reconstructing the continuous temporal waveform. Finally, post-synthesis artifact filtering and frame concatenation are applied to smooth inter-frame boundaries, mitigate blocking artifacts, and guarantee amplitude continuity across consecutive cardiac cycles.

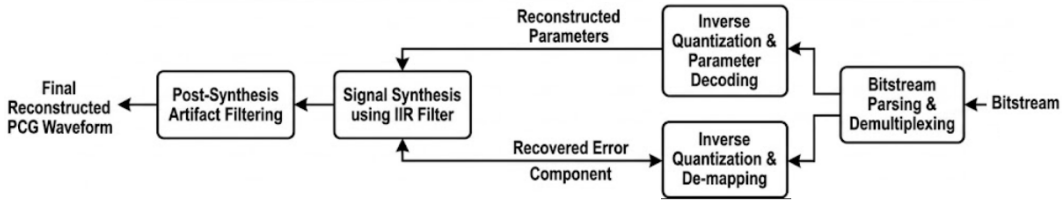


Figure 3. Decoder architecture and reconstruction stages

2.7. Prediction error encoding

The proposed system is tailored to perform PCG signal compression in an efficient manner with a target bit rate of few kbps according to the threshold parameter chosen. The representation of error components which are of utmost importance to the signal's diagnostic features is given priority, thereby maintaining high reconstruction fidelity. In addition to this, the residuals and the data that are kept are like they are compressed into a tiny dynamic range, and thus only 4-bit format is used to represent them. For each residual frame $e_m[n]$, the maximum absolute amplitude is first determined as $A_m = \max|e_m[n]|$. For a nonzero frame, the corresponding scaling exponent is determined by $\gamma_m = \lceil \log_2 A_m \rceil$, and the adaptive scale factor is selected as $S_m = 2^{\gamma_m}$, where $A_m \leq \mathrm{S_m}$. Each residual sample is then normalized using $u_m[n] = e_m[n]/S_m$ and expected to lie within $[-1,1]$.

A threshold $\mathrm{T_z}$ is subsequently applied to identify insignificant residual samples. A binary significance indicator is used to preserve their positions during decoding, while samples satisfying $|\mathrm{e_m[n]}| < \mathrm{T_z}$ are reconstructed as zero. The retained normalized samples are represented using a 4-bit uniform quantizer over $[-1,1]$, providing 16 quantization indices. The selected scaling exponent and significance information are transmitted as side information together with the quantized residual indices. At the decoder, the quantized values are dequantized and rescaled using $\hat{e}_m[n] = S_m\,\hat{u}_m[n]$, while the significance information restores the locations of the zero-valued samples. If $\mathrm{A_m} = 0$, the frame is represented by a dedicated zero-frame indication and no residual samples are transmitted. An overflow flag is reserved for exceptional cases in which $|\mathrm{u_m[n]}| > 1$, although such cases are avoided under the specified scaling rule. The system uses LSFs instead of raw LPC coefficients, because of the former's superior ability to withstand quantization effects. The thresholded residuals are compactly encoded with a 4-bit scheme after the scaling procedure previously explained, thus guaranteeing efficient representation of data while maintaining the same quality of the signal. A detailed overview of the scaling logic, range classification, and output mapping scheme is given in Table 1.

Table 1. Adaptive residual scaling and quantization

Scale code	Scaling exponent	Scale factor	Normalized residual range	Quantization method	Output mapping
000	γ_m	2^{γ_m}	$[-1,1]$	4-bit quantization	16 levels
001	$\gamma_m + 1$	2^{γ_m+1}	$[-1,1]$	4-bit quantization	16 levels
010	$\gamma_m + 2$	2^{γ_m+2}	$[-1,1]$	4-bit quantization	16 levels
011	$\gamma_m + 3$	2^{γ_m+3}	$[-1,1]$	4-bit quantization	16 levels
100	$\gamma_m + 4$	2^{γ_m+4}	$[-1,1]$	4-bit quantization	16 levels
101	$\gamma_m + 5$	2^{γ_m+5}	$[-1,1]$	4-bit quantization	16 levels
110	$\gamma_m + 6$	2^{γ_m+6}	$[-1,1]$	4-bit quantization	16 levels
111	$\gamma_m + 7$	2^{γ_m+7}	$[-1,1]$	4-bit quantization	16 levels
Zero-frame	-	-	-	$A_m = 0$	No residual data

2.8. Energy encoding and adaptive thresholding

This quantization method preserves the spectral accuracy required for the PCG reconstruction. The input is processed in short-time frames, where each one has *p* LPC parameters and error sequence. The bit rate is reduced by keeping only the loudest residual samples, which usually conserves 90% of the residual energy. The adaptive threshold is determined using the expression below, considering the signal's dynamic range:

$$\text{Threshold} = \theta = \alpha \times \max(|e[n]|) \quad (12)$$

where α is a scalar parameter in the range of [0, 1] which controls the sparsity level. Small amounts of α result in the best CR since less samples are kept but at the same time the quality of reconstruction is less. Besides the bits earmarked for the encoding of LSP coefficients, additional bits are used for the representation of the energy of the original frame. The energy value is then applied to properly scale the output signal of the reconstruction process. The method of adaptive thresholding is said to be very effective in the case of multi-pulse LPC systems, where the reduction of the number of non-zero residual components is crucial for obtaining high compression efficiency. The residual threshold controls the compromise between high compression performance and clinical waveform integrity. To investigate its effect, several threshold values were evaluated while keeping the remaining encoding parameters unchanged. Increasing the threshold value reduces the number of residual samples retained by the encoder and consequently improves the CR; however, excessive thresholding can increase reconstruction distortion. The best threshold value can be selected based on the observed balance between compression efficiency and signal fidelity.

3. RESULTS AND DISCUSSION

The PCG recordings used in this study were obtained from the PhysioNet/CinC Challenge 2016 database, which contains recordings from both normal and abnormal cardiac conditions. A total of 450 seconds of PCG recordings were selected for the compression experiments [4], [26]–[28], including recordings representing both normal and pathological heart sounds. Because the proposed compression scheme is a deterministic, frame-by-frame parametric signal-processing method that does not require data-driven training or weight optimization, the evaluated 450 seconds of PCG recordings, comprising both normal heart sounds and pathological murmurs from standard PhysioNet databases, provide a sufficient basis for proof-of-concept validation of reconstruction fidelity and compression performance. Two reconstruction methods were compared among them: one using the full (exact) residual signal, and the other applying a sparsified residual which was obtained through thresholding. This threshold was set to achieve a balanced compromise based on preliminary experimental analysis and its proven effectiveness in retaining key PCG features with a considerable reduction of data size.

The LPC parameters and the associated error sequence were generated during the analysis of each PCG frame. The residuals were either preserved without any alterations or their size was reduced by excluding the values lower than the specified threshold. The resultant data were structured into packets of predetermined size, which were specifically developed for low-bitrate transmission. When the decoder was used, the LPC coefficients and the residual parts were the means with which the waveforms that retained the clinically significant PCG features were created. Compared to many existing PCG compression techniques, the data transmission rate provided by the system is very impressive and thus the use of this system in real-time situations in resource-limited areas like wearables or remote diagnostic systems is justified. To quantify the storage reduction achieved by the encoding algorithm, the CR compares the raw, uncompressed payload capacity (Φ_{raw}) against the finalized encoded bit-stream size (Φ_{encoded}):

$$\text{CR} = \frac{\Phi_{\text{raw}}}{\Phi_{\text{encoded}}} \tag{13}$$

A larger CR means more efficient data compression, thus improving both storage capacity and transmission speed. Signal fidelity is evaluated holistically via the global signal-to-noise ratio (SNR). Let the benchmark physiological recording be represented as the discrete-time sequence c[n] and its synthesized counterpart as $\hat{c}[n]$, yielding the full-length reference vector $\text{c} = [c(1), c(2), \dots, c(N)]^{\text{T}}$ and the corresponding reconstruction error vector $\text{e} = [e(1), e(2), \dots, e(N)]^{\text{T}}$, where each element is defined by $e(n) = c(n) - \hat{c}(n)$. Using the empirical expectation operator E[·] to represent average signal power, the total SNR is formulated as (14):

$$\text{SNR}_{\text{global}} = 10 \log_{10} \left(\frac{E[c^2]}{E[e^2] + \sigma} \right) \tag{14}$$

where σ is a minute stabilization parameter (a strictly positive constant approaching zero) introduced to preclude undefined division-by-zero operations. Given the morphological non-stationarity of physiological waveforms, localized performance tracking is critical. The complete recording is partitioned into M disjoint analysis blocks of length L_s. For the m-th frame ($\text{m} = 1, 2, \dots, \text{M}$), let $\text{c}_\text{m} = \left[c_m[1], c_m[2], \dots, c_m[L_s]\right]^{\text{T}}$ designate the reference sub-vector and $\text{e}_\text{m} = \left[e_m[1], e_m[2], \dots, e_m[L_s]\right]^{\text{T}}$ denote the localized error sub-vector, with intra-frame elements $e_m[l] = c_m[l] - \hat{c}_m[l]$ for $l = 1, \dots, L_s$. The segmental SNR for frame m is determined by evaluating the ratio of localized signal energy to localized error variance:

$$\text{SNR}_m = 10 \log_{10} \left(\frac{E[\mathbf{c}_m^2]}{E[\mathbf{e}_m^2] + \sigma} \right) \tag{15}$$

The overarching mean objective quality across the entire clinical recording is subsequently aggregated by averaging these block-wise metrics [10]:

$$\overline{\text{SNR}} = \frac{1}{M} \sum_{m=1}^{M} \text{SNR}_m \tag{16}$$

The percent root mean square difference (PRD) serves as a rigorous clinical benchmark for structural deviation. Evaluated independently per segment using the frame-level vectors c_m and e_m to capture transient artifacts across individual cardiac cycles, the distortion index is expressed as (17):

$$\text{PRD}_m = \sqrt{\frac{E[\mathbf{e}_m^2]}{E[\mathbf{c}_m^2]}} \times 100 \quad (17)$$

Values approaching zero indicate near-lossless synthesis. The average segmental PRD over the complete recording is obtained by taking the arithmetic mean of the frame-level PRD values [10]:

$$\overline{\text{PRD}} = \frac{1}{M}\sum_{m=1}^{M} \text{PRD}_m \quad (18)$$

In general, lower PRD values indicate greater similarity between the reference and recovered waveforms. In this study, PRD is rigorously evaluate the balance between bit reduction and waveform fidelity under different residual-threshold settings. The PRD results provide evidence of signal-level fidelity; however, they should not be interpreted as a substitute for clinical validation or as direct evidence of diagnostic equivalence. The evaluation of LPC-based PCG compression with sparse residual representation was performed on a short-time frame under two experimental conditions: one using the entire residual and the other applying residual thresholding. The results shown in Figure 4 indicate that both reconstruction methods are very similar to the original waveform. The thresholder residual effectively retained important morphological features while greatly reducing data volume, thus confirming the method's reliability in clinical applications. This preliminary study did not include the assessment of inter-observer variability. The results suggested that the approach strikes a good balance between compression rate and signal quality, which makes it suitable for low-bitrate systems like wearable medical sensors and IoT-enabled systems. Conventional or residual energy consists mainly of the few dominant impulses. The thresholder residual maintains temporal and amplitude characteristics that are important for the original signal, thus presenting a compressed version that would not affect the reconstruction quality at all. The experiments confirm that the compression method keeps the characteristic PCG morphology whether it is a short or long recording, meanwhile, highly reducing the data size by means of sparse residual representation.

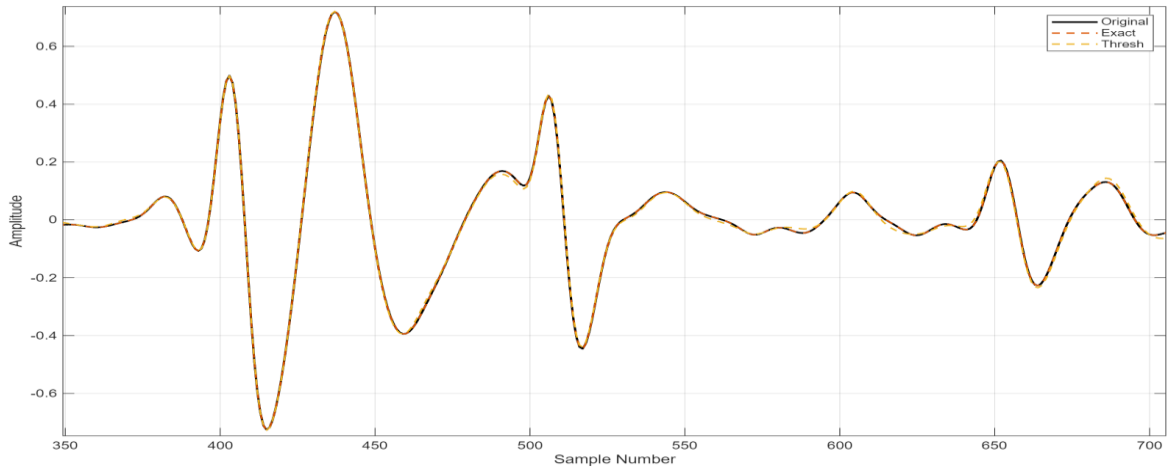


Figure 4. Comparison of original and predicted PCG signals using exact and sparsified residuals, illustrating the reduction in data size while preserving signal morphology

As presented in Table 2, PRD increases from 0% for the exact-residual representation to 7.8% at a threshold of 10^{-4}, while the CR simultaneously scales from 4: 1 to 29.84: 1. This quantitative progression reflects the fundamental trade-off between bitstream sparsity and signal reconstruction fidelity. At lower bitrates, the algorithm aggressively truncates low-magnitude residual components, concentrating bit allocation entirely on clinically salient waveform dynamics. Importantly, while the PRD remains strictly within acceptable bounds across the investigated thresholds, PRD alone cannot serve as an absolute measure of clinical fidelity. Comprehensive clinical validation ultimately requires evaluation against annotated diagnostic databases and expert morphological review. Furthermore, this multi-tier performance demonstrates that the proposed framework offers tunable operational modes, ranging from near-lossless fidelity at high SNR for critical telemetry to ultra-low bitrates for resource-constrained, long-term wearable monitoring. To contextualize these performance characteristics within the broader state of the art, the proposed approach was benchmarked against the primary classes of biomedical signal compression:

- Time-domain techniques: classical algorithms such as differential pulse code modulation (DPCM), amplitude zone time epoch coding (AZTEC), and turning point (TP) [34], [35] exhibit minimal computational complexity suitable for legacy microcontrollers. However, because they operate strictly on instantaneous amplitude variations without exploiting spectral redundancy, their performance is inherently bounded (CR $\approx$ 3-10: 1; PRD $\approx$ 4%-8%).
- Transform-domain methods: orthogonal decomposition schemes, including the discrete wavelet transform (DWT), discrete cosine transform (DCT), and karhunen-loève transform (KLT) [35], [36], significantly enhance energy compaction by decoupling non-stationary spectral components (CR $\approx$ 10-20: 1; PRD $\approx$ 3%-6%). Nonetheless, transform-only methodologies leave residual temporal correlations unmodeled across transform sub-bands, restricting further efficiency gains.
- Deep learning (DL) and autoencoder frameworks: recent deep neural network and convolutional autoencoder architectures [37] have achieved exceptional accuracy (PRD $\leq$ 2%). Despite their representational power, deep architectures introduce prohibitive computational and memory footprints, require substantial pre-training datasets, and face generalizability risks when encountering unseen patient morphologies or motion artifacts, rendering them impractical for ultra-low-power edge nodes.
- Compressed sensing (CS): CS paradigms [38], [39] leverage sub-Nyquist sampling and domain sparsity to attain high CR $\approx$ 10-25: 1. However, the signal recovery phase relies heavily on iterative convex optimization algorithms, imposing substantial computational latency and dynamic power penalties at the receiving terminal.

In contrast, the proposed framework establishes a deterministic, non-iterative formulation that bridges the gap between predictive modeling and sparse representation. By achieving CR spanning 4: 1 to nearly 30: 1 alongside preserved waveform fidelity (PRD $\leq$ 7.8%) without requiring hardware accelerators, intensive training, or iterative recovery solvers, the proposed method provides a highly viable and energy-efficient solution for real-time cardiac telemonitoring, edge wearables, and IoT-driven healthcare ecosystems.

Table 2. Rate-distortion performance of the proposed LPC-based PCG compression scheme across varying residual threshold levels

Method	Threshold θ	$\overline{\text{PRD}}$ (%)	$\text{SNR}_{\text{global}}$ (dB)	$\overline{\text{SNR}}$ (dB)	CR
Exact residual	0	0	80.12	Very high	4:1
Sparse residual	2×10^{-5}	0.8	47.87	67.33	3.22:1
Sparse residual	4×10^{-5}	2.3	32.83	47.17	7.32:1
Sparse residual	8×10^{-5}	5.4	22.86	30.91	20.98:1
Sparse residual	10^{-4}	7.8	14.58	16.09	29.84:1

4. CONCLUSION

This study presented an LPC-based PCG signal compression framework combining adaptive residual thresholding, LSF parameter quantization, and selective residual encoding. Experimental results demonstrated flexible CR from 4:1 to 30:1 while preserving critical diagnostic morphology and high signal fidelity, confirming its viability for real-time, resource-constrained IoT telemedicine platforms and wearable cardiac monitoring. Limitations include the size and diversity of the evaluation dataset and the absence of embedded hardware implementation. Future work will validate the method on larger, multi-center datasets with diverse valvular pathologies and investigate real-time embedded implementation to establish broader clinical applicability.

FUNDING INFORMATION

This work was funded by the American University of The Middle East, Kuwait and by a grant from Aeon Medical Supplies Company, Jordan.

AUTHOR CONTRIBUTIONS STATEMENT

This journal uses the Contributor Roles Taxonomy (CRediT) to recognize individual author contributions, reduce authorship disputes, and facilitate collaboration.

Name of Author	C	M	So	Va	Fo	I	R	D	O	E	Vi	Su	P	Fu
Samer Alabed	✓	✓	✓	✓	✓	✓	✓	✓	✓	✓	✓	✓	✓	✓
Mohammad Al-Rabayah		✓		✓		✓		✓		✓	✓	✓	✓	✓
Omar M. Bwaliez		✓		✓		✓	✓			✓	✓		✓	

C : **C**onceptualization
M : **M**ethodology
So : **So**ftware
Va : **Va**lidation
Fo : **Fo**rmal analysis
I : **I**nvestigation
R : **R**esources
D : **D**ata Curation
O : Writing - **O**riginal Draft
E : Writing - Review & **E**diting
Vi : **Vi**sualization
Su : **Su**pervision
P : **P**roject administration
Fu : **Fu**nding acquisition

CONFLICT OF INTEREST STATEMENT

Authors state no conflict of interest.

DATA AVAILABILITY

The datasets analyzed in this study are publicly available.

REFERENCES

[1] R. Prasad, G. Yilmaz, O. Chetelat, and M. Magimai-Doss, "Detection of S1 And S2 locations in phonocardiogram signals using zero frequency filter," in *ICASSP 2020 - 2020 IEEE International Conference on Acoustics, Speech and Signal Processing (ICASSP)*, May 2020, pp. 1254–1258, doi: 10.1109/ICASSP40776.2020.9053155.

[2] M. Nath, S. Srivastava, N. Kulshrestha, and D. Singh, "Detection and localization of S 1 and S 2 heart sounds by 3rd order normalized average Shannon energy envelope algorithm," in *Proceedings of the Institution of Mechanical Engineers, Part H: Journal of Engineering in Medicine*, vol. 235, no. 6, pp. 615–624, Jun. 2021, doi: 10.1177/0954411921998108.

[3] J. Burns, M. Ganigara, and A. Dhar, "Application of intelligent phonocardiography in the detection of congenital heart disease in pediatric patients: A narrative review," *Progress in Pediatric Cardiology*, vol. 64, no. 1, p. 101455, Mar. 2022, doi: 10.1016/j.ppedcard.2021.101455.

[4] B. Zhu, Z. Zhou, S. Yu, X. Liang, Y. Xie, and Q. Sun, "Review of phonocardiogram signal analysis: Insights from the PhysioNet/CinC Challenge 2016 database," *Electronics*, vol. 13, no. 16, Aug. 2024, doi: 10.3390/electronics13163222.

[5] S. Samant and A. Dixit, "Phonocardiogram (PCG) in cardiac diagnostics: A comprehensive review of acquisition, signal processing, machine learning, and clinical applications," in *2026 International Conference on Signal, Systems, and Computing for Next-Gen Automation (ICSSCNA)*, May 2026, pp. 166–171, doi: 10.1109/ICSSCNA68616.2026.11547150.

[6] F. Javed, J. Flood, D. Tellez, and R. Kirkpatrick, "Remote patient monitoring system based on wireless wearable chest patch," in *2024 46th Annual International Conference of the IEEE Engineering in Medicine and Biology Society (EMBC)*, Jul. 2024, pp. 1–4, doi: 10.1109/EMBC53108.2024.10782729.

[7] P. Kumar, P. Singh, K. Sagar, and N. R. Roy, "Heart disease detection using phonocardiogram and IoT devices: A comparative literature review," in *2026 International Conference on Intelligent Systems in Engineering, Secured Systems and Cybersecurity (ICISESSC)*, Apr. 2026, pp. 360–365, doi: 10.1109/ICISESSC68634.2026.11542621.

[8] D. Ragusa *et al.*, "Ultraefficient compressed phonocardiogram classification on a custom embedded neural accelerator," *IEEE Internet of Things Journal*, vol. 13, no. 4, pp. 6485–6494, Feb. 2026, doi: 10.1109/JIOT.2025.3635785.

[9] B. M. Mahmmod *et al.*, "Patient Monitoring System Based on Internet of Things: A Review and Related Challenges With Open Research Issues," *IEEE Access*, vol. 12, pp. 132444-132479, 2024, doi: 10.1109/ACCESS.2024.3455900.

[10] S. Alabed, M. Al-Rabayah, O. M. Bwaliez, and S. A. Hasan, "Efficient ECG signal coding with interpolation-enhanced LPC for telehealth and wearable devices," *e-Prime – Nexus of Electrical, Electronic, and Intelligent Engineering*, vol. 17, Sep. 2026, doi: 10.1016/j.eprime.2026.201162.

[11] M. M. Rodgers, V. M. Pai, and R. S. Conroy, "Recent Advances in Wearable Sensors for Health Monitoring," *IEEE Sensors Journal*, vol. 15, no. 6, pp. 3119-3126, June 2015, doi: 10.1109/JSEN.2014.2357257.

[12] G. Hassan, K. M. Hosny, M. M. Fouda, and I. S. Fathi, "Efficient compression of fetal phonocardiography bio-medical signals for internet of healthcare things," *IEEE Access*, vol. 11, pp. 122991–123003, 2023, doi: 10.1109/ACCESS.2023.3329889.

[13] R. McAulay and T. Quatieri, "Speech analysis/synthesis based on a sinusoidal representation," *IEEE Transactions on Acoustics, Speech, and Signal Processing*, vol. 34, no. 4, pp. 744–754, Aug. 1986, doi: 10.1109/TASSP.1986.1164910.

[14] S. Ahmadi and A. S. Spanias, "New techniques for sinusoidal coding of speech at 2400 bps," in *Conference Record of The Thirtieth Asilomar Conference on Signals, Systems and Computers*, 1996, vol. 1, pp. 770–774, doi: 10.1109/ACSSC.1996.601158.

[15] J. Jensen, S. H. Jensen, and E. Hansen, "Harmonic exponential modeling of transitional speech segments," in *2000 IEEE International Conference on Acoustics, Speech, and Signal Processing. Proceedings (Cat. No.00CH37100)*, 2000, vol. 3, pp. 1439–1442, doi: 10.1109/ICASSP.2000.861884.

[16] R. Vafin, S. V. Andersen, and W. B. Kleijn, "Exploiting time and frequency masking in consistent sinusoidal analysis-synthesis," in *2000 IEEE International Conference on Acoustics, Speech, and Signal Processing. Proceedings (Cat. No.00CH37100)*, 2000, vol. 2, pp. II901–II904, doi: 10.1109/ICASSP.2000.859106.

[17] S. K. Ghosh, A. Ray, R. K. Tripathy, and P. R. N, "A transform domain approach for the compression of fetal phonocardiogram signal," *IEEE Sensors Letters*, vol. 5, no. 5, pp. 1–4, May 2021, doi: 10.1109/LSENS.2021.3074985.

[18] H. Naseri and M. R. Homaeinezhad, "Detection and boundary identification of phonocardiogram sounds using an expert frequency-energy based metric," *Annals of Biomedical Engineering*, vol. 41, no. 2, pp. 279–292, Feb. 2013, doi: 10.1007/s10439-012-0645-x.

[19] P. T. Krishnan, P. Balasubramanian, and S. Umapathy, "Automated heart sound classification system from unsegmented

phonocardiogram (PCG) using deep neural network," *Physical and Engineering Sciences in Medicine*, vol. 43, no. 2, pp. 505–515, Jun. 2020, doi: 10.1007/s13246-020-00851-w.
[20] T. Gao, L. Jiang, X. Wang and L. Qiu, "Acoustic Signal Compression Research Based on Wavelet and Compressed Sensing," in *2021 IEEE International Conference on Power Electronics, Computer Applications (ICPECA)*, Shenyang, China, 2021, pp. 777-782, doi: 10.1109/ICPECA51329.2021.9362686.
[21] R. McAulay and T. Quatieri, "Magnitude-only reconstruction using a sinusoidal speech modelMagnitude-only reconstruction using a sinusoidal speech model," in *ICASSP '84. IEEE International Conference on Acoustics, Speech, and Signal Processing*, 1984, vol. 9, pp. 441–444, doi: 10.1109/ICASSP.1984.1172492.
[22] R. Mcaulay and T. Quatieri, "Phase modelling and its application to sinusoidal transform coding," in *ICASSP '86. IEEE International Conference on Acoustics, Speech, and Signal Processing*, 1986, vol. 11, pp. 1713–1716, doi: 10.1109/ICASSP.1986.1169250.
[23] C. Xu *et al*., "Hearing heartbeat from voice," in *Proceedings of the 20th ACM Conference on Embedded Networked Sensor Systems*, Nov. 2022, pp. 149–163, doi: 10.1145/3560905.3568508.
[24] T. H. Chowdhury, K. N. Poudel, and Y. Hu, "Time-frequency analysis, denoising, compression, segmentation, and classification of PCG signals," *IEEE Access*, vol. 8, pp. 160882–160890, 2020, doi: 10.1109/ACCESS.2020.3020806.
[25] H. Namazi and O. Krejcar, "Analysis of pregnancy development by complexity and information-based analysis of fetal phonocardiogram (PCG) signals," *Fluctuation and Noise Letters*, vol. 20, no. 04, Aug. 2021, doi: 10.1142/S0219477521500280.
[26] A. K. Abbas and R. Bassam, *Phonocardiography signal processing*. Cham: Springer International Publishing, 2009, doi: 10.1007/978-3-031-01637-0.
[27] A. Thalmayer, S. Zeising, G. Fischer, and J. Kirchner, "A robust and real-time capable envelope-based algorithm for heart sound classification: validation under different physiological conditions," *Sensors*, vol. 20, no. 4, pp. 972–992, Feb. 2020, doi: 10.3390/s20040972.
[28] M. M. Bassiouni, I. Hegazy, N. Rizk, E.-S. A. El-Dahshan, and A. M. Salem, "Combination of ECG And PPG signals for smart HealthCare systems: Techniques, applications, and challenges," in *2021 Tenth International Conference on Intelligent Computing and Information Systems (ICICIS)*, Dec. 2021, pp. 448–455, doi: 10.1109/ICICIS52592.2021.9694241.
[29] M. Chowdhury, K. Poudel, and Y. Hu, "Phonocardiography Data Compression Using Discrete Wavelet Transform," in *IEEE Signal Processing in Medicine and Biology Symposium (SPMB)*, Philadelphia, PA, USA, 2018, pp. 01-03, doi: 10.1109/SPMB.2018.8615617.
[30] S. Ardhapurkar, R. Manthalkar, and S. Gajre, "Electrocardiogram compression by linear prediction and wavelet sub-band coding techniques," in *2011 Computing in Cardiology*, 2011, pp. 141–144.
[31] L. Wang, J. Belina, A. Vasinonta, M. Berner, and S. Ramprashad, "Compression of ECG using a code excited linear prediction (CELP)," in *Proceedings of 16th Annual International Conference of the IEEE Engineering in Medicine and Biology Society*, 1994, pp. 1264–1265, doi: 10.1109/IEMBS.1994.415424.
[32] R. A. George and R. Periyasamy, "Modelling of electrocardiogram using autoregressive moving average model and linear predictive coefficient a comparative study," in *2021 Seventh International conference on Bio Signals, Images, and Instrumentation (ICBSII)*, Mar. 2021, pp. 1–4, doi: 10.1109/ICBSII51839.2021.9445142.
[33] M. Jia, F. Li, Y. Pu, and Z. Chen, "A lossless electrocardiogram compression system based on dual-mode prediction and error modeling," *IEEE Access*, vol. 8, pp. 101153–101162, 2020, doi: 10.1109/ACCESS.2020.2998608.
[34] A. Dhanusha, V. Singh, S. Bharadwaj, B. Shrehari, V. S. Gummaraju, and T. Badgeri, "VLSI implementation of lossless ECG compression using modified GRE and RLC," in *2025 6th International Conference on Electronics and Sustainable Communication Systems (ICESC)*, Sep. 2025, pp. 352–357, doi: 10.1109/ICESC65114.2025.11212258.
[35] P. Tripathi *et al.*, "A comparative analysis on 1D & 2D ECG applying data compression approaches," in *2023 International Conference on Artificial Intelligence and Smart Communication (AISC)*, Jan. 2023, pp. 261–266, doi: 10.1109/AISC56616.2023.10085223.
[36] A. Cerca, A. Lourenco, and A. Ferreira, "A study on compression techniques for off-the-person electrocardiogram signals," in *2019 IEEE 6th Portuguese Meeting on Bioengineering (ENBENG)*, Feb. 2019, pp. 1–4, doi: 10.1109/ENBENG.2019.8692467.
[37] T. Bekiryazıcı, G. Aydemir, and H. Gürkan, "Electrocardiogram signal compression using deep convolutional autoencoder with constant error and flexible compression rate," *IRBM*, vol. 45, no. 6, Dec. 2024, doi: 10.1016/j.irbm.2024.100859.
[38] H. Mamaghanian, N. Khaled, D. Atienza, and P. Vandergheynst, "Compressed sensing for real-time energy-efficient ECG compression on wireless body sensor nodes," *IEEE Transactions on Biomedical Engineering*, vol. 58, no. 9, pp. 2456–2466, Sep. 2011, doi: 10.1109/TBME.2011.2156795.
[39] L. F. Polania, R. E. Carrillo, M. Blanco-Velasco, and K. E. Barner, "Exploiting prior knowledge in compressed sensing wireless ECG systems," *IEEE Journal of Biomedical and Health Informatics*, vol. 19, no. 2, pp. 508–519, Mar. 2015, doi: 10.1109/JBHI.2014.2325017.

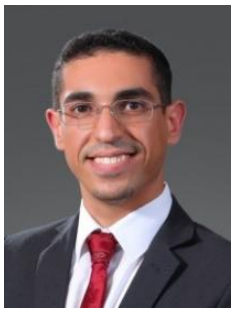
BIOGRAPHIES OF AUTHORS



Samer Alabed is a professor of Electrical and Biomedical Engineering at the German Jordanian University (GJU), a Strategic Academic Leader, and an expert in Signal Processing, Internet of Things, and Artificial Intelligence. Throughout his tenure at GJU, he has held several key academic and administrative leadership positions, including head of Department of Biomedical Engineering, Exchange Coordinator for the German Year Program, director of the Department of Accreditation and Quality Assurance, and director of the Department of E-Learning and Academic Performance Improvement. Prior to joining GJU, he served as an associate professor at the American University of the Middle East, Kuwait, from 2015 to 2022. He earned his Ph.D. in Electrical Engineering and Information Technology from TU-Darmstadt, Germany. From 2008 to 2015, he was also affiliated with TU Darmstadt, where he contributed to academic and research activities in electrical engineering, with a focus on digital signal processing and related technologies. He can be contacted at email: Samer.Alabed@gju.edu.jo.



Mohammad Al-Rabayah earned his Ph.D. in Electrical Engineering from University of New South Wales. He is serving as an associate professor at American University of the Middle East (AUM), where he teaches a variety of courses, advises students, and contributes to departmental excellence. He was an assistant professor at Prince Sultan University. During his tenure, he taught courses in the Department of Communication and Networks and played a key role in supporting the university's efforts to achieve ABET accreditation. He can be contacted at email: Mohammad.Alrabayah@aum.edu.kw.



Dr. Omar M. Bwaliez is a professor at the Department of Management Sciences the Business School at the German Jordanian University (GJU), where he also serves as dean's assistant for accreditation and quality assurance. With over a decade of experience, he has excelled in teaching, research, training, and consultancy across various universities and companies in the Middle East and Europe. His scholarly contributions are reflected in numerous peer-reviewed articles featured in prestigious journals indexed by Scopus and Web of Science. He also holds multiple professional certifications in the fields of engineering management, Industry 4.0 technologies, quality management, higher education institutions assessment, and innovation. Prior to his academic career, he held key positions in Jordan's manufacturing sector, including industrial engineer, business development engineer, and quality assurance manager. He can be contacted at email: Omar.Bwaliez@gju.edu.jo.